Chapter 15

Quantum Structured Solar Cells

A.J. Nozik[a,b]

[a]Center for Basic Sciences, National Renewable Energy Laboratory, 1617 Cole Blvd., Golden, CO 80401, USA
[b]Department of Chemistry, University of Colorado, Boulder, CO 80309, USA

1. INTRODUCTION

The cost of delivered photovoltaic (PV) power is determined by the PV module conversion efficiency and the capital cost of the PV system per unit area. To achieve very low cost PV power, it is necessary to develop cells that have very high conversion efficiency and moderate cost. Toward this end, we have been investigating the possibility of achieving high conversion efficiency in single-bandgap solar cells by capturing the excess energy of electron – hole pairs created by the absorption of solar photons larger than the bandgap to do useful work before these high-energy electron – hole pairs convert their excess kinetic energy (equal to the difference between the photogenerated electron energy and the conduction band energy) to heat through phonon emission [1–4]. These highly excited electrons and holes are termed hot electrons and hot holes (or hot carriers); in semiconductor nanocrystals, the photogenerated electron – hole pairs are correlated and are termed excitons. Semiconductor nanocrystals (also called quantum dots, QDs) have discrete electronic states, and the absorption of photons with energies greater than the energy difference between the highest hole state ($1 S_h$) and the lowest electron state ($1 S_e$) (also termed the HOMO-LUMO transition) produces excited excitons.

The extraction of useful work from hot electron – hole pairs (hot carriers) is difficult in bulk semiconductors because the cooling process that occurs through inelastic carrier–phonon scattering and subsequent hot-carrier cooling is very fast (sub-ps). However, the formation of discrete quantized levels in QDs affects the relaxation and cooling dynamics of high-energy excitons and this could enhance the power conversion efficiency by either using the excess energy of excited excitons to create additional excitons (a process
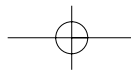
1   termed "multiple exciton generation, MEG" [5]), or allowing electrical or
2   chemical free energy to be extracted from the excited excitons through charge
3   separation before the excitons relax and produce heat.

4   As is well known, the maximum thermodynamic efficiency for the
5   conversion of unconcentrated solar irradiance into electrical free energy in
6   the radiative limit, assuming detailed balance, a single threshold absorber,
7   a maximum yield of one electron–hole pair per photon, and thermal equi-
8   librium between electrons and phonons, was calculated by Shockley and
9   Queisser in 1961 [6] to be about 31%; this analysis is also valid for the con-
10 version to chemical free energy [7, 8]. This efficiency is attainable in semi-
11 conductors with bandgaps ranging from about 1.2 to 1.4 eV.

12   However, the solar spectrum contains photons with energies ranging
13 from about 0.5 to 3.5 eV. Photons with energies below the semiconductor
14 bandgap are not absorbed, while those with energies above the bandgap create
15 electrons and holes (charge carriers) with a total excess kinetic energy equal to
16 the difference between the photon energy and the bandgap. This excess kinetic
17 energy creates an effective temperature for an ensemble of photogenerated
18 carriers that can be much higher than the lattice temperature; such carriers
19 are called "hot electrons and hot holes," and their initial temperature upon pho-
20 ton absorption can be as high as 3000°K with the lattice temperature at 300°K.
21 In bulk semiconductors, the division of this kinetic energy between electrons
22 and holes is determined by their effective masses, with the carrier having the
23 lower effective mass receiving more of the excess energy [1]. Thus,

$$\Delta E_e = (h\nu - E_g)[1 + m_e^*/m_h^*]^{-1} \tag{1}$$

$$\Delta E_h = (h\nu - E_g) - \Delta E_e \tag{2}$$

28 where E_e is the energy difference between the conduction band and the ini-
29 tial energy of the photogenerated electron, and E_h the energy difference
30 between the valence band and the photogenerated hole (see Fig. 1). However,
31 in QDs, the distribution of excess energy is determined by the quantized
32 energy level structure in the QDs and the associated selection rules for the
33 optical transitions between the hole and electron levels [9].

34   In the Shockley–Queisser analysis, a major factor limiting the conversion
35 efficiency to 31% is that the absorbed photon energy above the semicon-
36 ductor bandgap is lost as heat through electron–phonon scattering and sub-
37 sequent phonon emission, as the carriers relax to their respective band edges
38 (bottom of conduction band for electrons and top of valence band for holes)
39 (see Fig. 1) and equilibrate with the phonons. The main approach to reduce
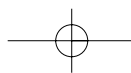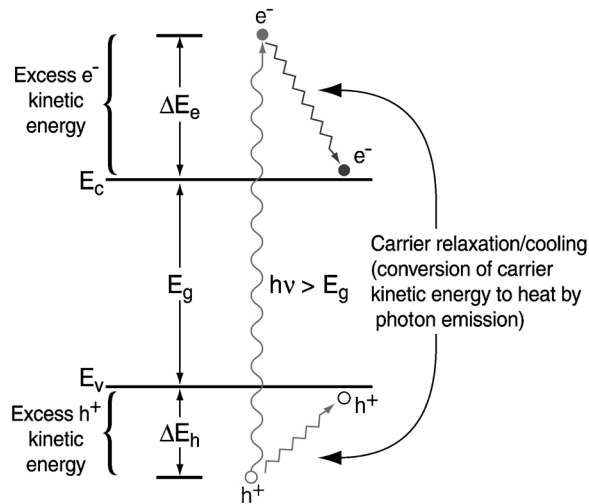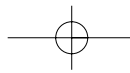
Fig. 1. Hot carrier relaxation/cooling dynamics in semiconductors.

this loss and increase efficiency above the 31% limit has been to use a stack of cascaded multiple p–n junctions in the absorber with bandgaps better matched to the solar spectrum; in this way higher-energy photons are absorbed in the higher-bandgap semiconductors and lower-energy photons in the lower-bandgap semiconductors, thus reducing the overall heat loss due to carrier relaxation via phonon emission. In the limit of an infinite stack of bandgaps perfectly matched to the solar spectrum, the ultimate conversion efficiency at one-sun intensity increases to about 66%. For practical purposes, the stacks have been limited to two or three p–n junctions; actual efficiencies of about 32% have been reported in PV cells with two cascaded p–n junctions. Other approaches to exceed the Shockley–Queisser limit include hot carrier solar cells [1–3], solar cells producing multiple electron–hole pairs per photon [10–14], multiband and impurity solar cells [12, 15], and thermo-PV/thermophotonic cells [12]. Here, we will only discuss hot carrier and MEG solar cells, and the effects of size quantization in semiconductor QDs on the carrier dynamics that control the probability of these processes.

There are two fundamental ways to utilize hot carriers or hot excitons for enhancing the efficiency of photon conversion. One way produces an enhanced photovoltage, and the other way produces an enhanced photocurrent. The former requires that the carriers be extracted from the photoconverter before they cool [2, 3], while the latter requires the energetic hot carriers to produce a second (or more) electron–hole pair through MEG – a process that is the inverse
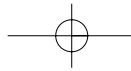
1   of an Auger process whereby two electron–hole pairs recombine to produce a
2   single highly energetic electron–hole pair. In order to achieve the former, the
3   rates of photogenerated-carrier separation, transport, and interfacial transfer
4   across the semiconductor interface must all be fast compared to the rate of
5   carrier cooling [3, 4, 16, 17]. The latter requires that the rate of exciton multi-
6   plication is greater than the rate of carrier cooling and forward Auger processes.
7   Hot electrons and hot holes generally cool at different rates because they
8   generally have different effective masses; for most inorganic semiconductors
9   electrons have effective masses that are significantly lighter than holes and
10   consequently cool more slowly. Another important factor is that hot-carrier
11   cooling rates are dependent upon the density of the photogenerated-hot
12   carriers (viz, the absorbed light intensity) [18–20]. Here, most of the dynam-
13   ical effects we will discuss are dominated by electrons rather than holes;
14   therefore, we will restrict our subsequent discussion primarily to the relax-
15   ation dynamics of photogenerated electrons.
16   Finally, in recent years it has been proposed [3, 4, 16, 21–24] and exper-
17   imentally verified in some cases [1, 25–27], that the relaxation dynamics of
18   photogenerated carriers may be markedly affected by quantization effects in
19   the semiconductor (i.e., in semiconductor quantum wells (QWs), quantum
20   wires, QDs, superlattices, and nanostructures). That is, when the carriers in
21   the semiconductor are confined by potential barriers to regions of space that
22   are smaller than or comparable to their deBroglie wavelength or to the Bohr
23   radius of excitons in the semiconductor bulk, the relaxation dynamics can be
24   dramatically altered; specifically the hot-carrier cooling rates may be drama-
25   tically reduced, and the rate of producing multiple excitons per photon could
26   become competitive with the rate of carrier cooling [1] (see Fig. 2).

2. RELAXATION DYNAMICS OF HOT CARRIERS IN
BULK SEMICONDUCTORS

31   Upon photoexcitation with a laser pulse, the initial carrier distributions are
32   usually not Boltzmann-like, and the first step toward establishing equilibrium
33   is for the hot carriers to interact separately among themselves and with the ini-
34   tial population of cold carriers through their respective carrier–carrier colli-
35   sions and inter-valley scattering to form separate Boltzmann distributions of
36   electrons and holes. These two Boltzmann distributions can then be separately
37   assigned an electron and hole temperature that reflects the distributions of
38   kinetic energy in the respective charge carrier populations. If photon absorp-
39   tion produces electrons and holes with initial excess kinetic energies at least
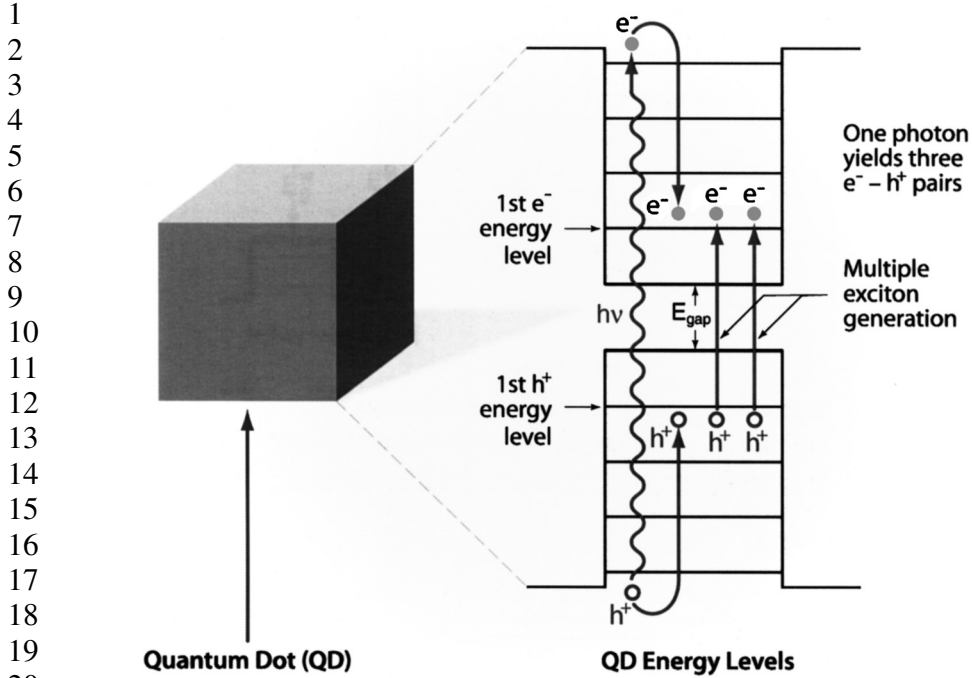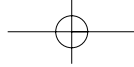
Fig. 2. Enhanced PV efficiency in QD solar cells by MEG (inverse Auger effect).

kT above the conduction and valence bands, respectively, then both initial carrier temperatures are always above the lattice temperature and the carriers are called hot carriers. This first stage of relaxation or equilibration occurs very rapidly ($<100\,fs$) [18, 19], and this process is often referred to as carrier thermalization (i.e., formation of a thermal distribution described by Boltzmann statistics).

After the separate electron and hole populations come to equilibrium among themselves in less than $100\,fs$, they are still not yet in equilibrium with the lattice. The next step of equilibration is for the hot electrons and hot holes to equilibrate with the semiconductor lattice. The lattice temperature is the ambient temperature and is lower than the initial hot electron and hot hole temperatures. Equilibration of the hot carriers with the lattice is achieved through carrier–phonon interactions (phonon emission) whereby the excess kinetic energy of the carriers is transferred from the carriers to the phonons; the phonons involved in this process are the longitudinal optical (LO) phonons. This may occur by each carrier undergoing separate interactions with the phonons, or in an Auger process where the excess energy of one carrier type
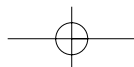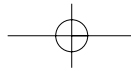
1   is transferred to the other type, which then undergoes the phonon interaction.
2   The phonon emission results in cooling of the carriers and heating of the lat-
3   tice until the carrier and lattice temperatures become equal. This process is
4   termed carrier cooling, but some researchers also refer to it as thermaliza-
5   tion; however, this latter terminology can cause confusion with the first stage
6   of equilibration that just establishes the Boltzmann distribution among the
7   carriers. Here, we will restrict the term thermalization to the first stage of
8   carrier relaxation, and we will refer to the second stage as carrier cooling
9   (or carrier relaxation) through carrier–phonon interactions.
10   The final stage of equilibration results in complete relaxation of the
11   system; the electrons and holes can recombine, either radiatively or non-
12   radiatively, to produce the final electron and hole populations that existed in
13   equilibrium in the dark before photoexcitation. Another important possible
14   pathway following photoexcitation of semiconductors is for the photogen-
15   erated electrons and holes to undergo spatial separation. Separated photogen-
16   erated carriers can subsequently produce a photovoltage and a photocurrent
17   (PV effect) [28–30]; alternatively, the separated carriers can drive electro-
18   chemical oxidation and reduction reactions (generally labeled redox reactions)
19   at the semiconductor surface (photoelectrochemical energy conversion) [31].
20   These two processes form the basis for devices/cells that convert radiant
21   energy (e.g., solar energy) into electrical [28–30] or chemical-free energy
22   (PV cells and photoelectrochemical cells, respectively) [31].

2.1. Quantum Wells and Superlattices

25   Semiconductors show dramatic quantization effects when charge carriers
26   are confined by potential barriers to small regions of space where the dimen-
27   sions of the confinement are less than their deBroglie wavelength; the length
28   scale at which these effects begin to occur range from about 10 to 50 nm for
29   typical semiconductors (Groups IV, III–V, II–VI). In general, charge carriers
30   in semiconductors can be confined by potential barriers in one spatial dimen-
31   sion, two spatial dimensions, or in three spatial dimensions. These regimes are
32   termed quantum films, quantum wires, and QDs, respectively. Quantum films
33   are also more commonly referred to simply as QWs.
34   One-dimensional QWs, hereafter called quantum films or just QWs, are
35   usually formed through epitaxial growth of alternating layers of semiconductor
36   materials with different bandgaps. A single QW is formed from one semicon-
37   ductor sandwiched between two layers of a second semiconductor having a
38   larger bandgap; the center layer with the smaller bandgap semiconductor forms
39   the QW while the two layers sandwiching the center layer create the potential
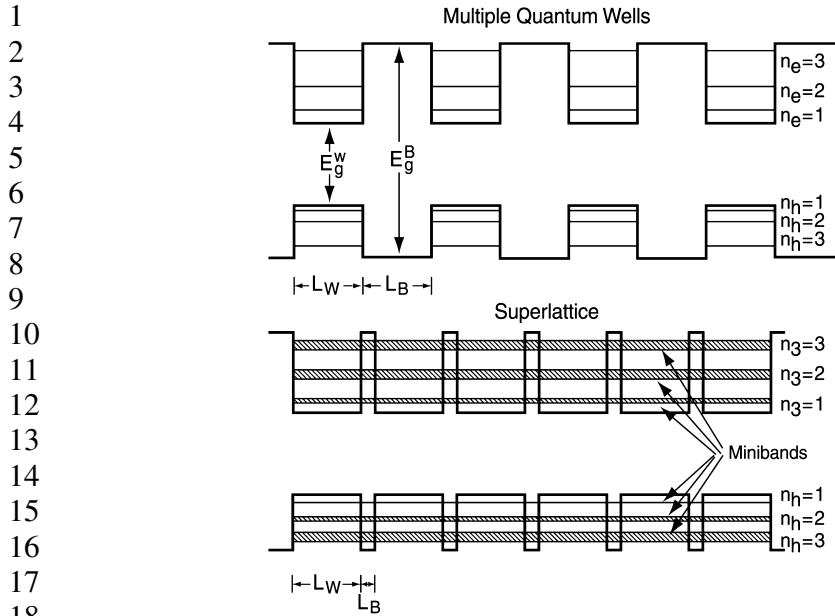
Fig. 3. Difference in electronic states between MQW structures (barriers $>40\,\text{Å}$) and superlattices (barriers $<40\,\text{Å}$); miniband formation occurs in the superlattice structure, which permits carrier delocalization.

barriers. Two potential wells are actually formed in the QW structure; one well is for conduction-band electrons, the other for valence-band holes. The well depth for electrons is the difference (i.e., the offset) between the conduction-band edges of the well and barrier semiconductors, while the well depth for holes is the corresponding valence band offset. If the offset for either the conduction or valence bands is zero, then only one carrier will be confined in a well.

Multiple QW (MQW) structures consist of a series of QWs (i.e., a series of alternating layers of wells and barriers). If the barrier thickness between adjacent wells prevents significant electronic coupling between the wells, then each well is electronically isolated; this type of structure is termed a MQW. On the other hand, if the barrier thickness is sufficiently thin to allow electronic coupling between wells (i.e., there is significant overlap of the electronic wavefunctions between wells), then the electronic charge distribution can become delocalized along the direction normal to the well layers. This coupling also leads to a broadening of the quantized electronic states of the wells; the new broadened and delocalized quantized states are termed *minibands* (see Fig. 3). A MQW structure that exhibits strong electronic

1   coupling between the wells is termed a *superlattice*. The critical thickness
2   at which miniband formation just begins to occur is about 40 Å [32, 33]; the
3   electronic coupling increases rapidly with decreasing thickness and mini-
4   band formation is very strong below 20 Å [32]. Superlattice structures yield
5   efficient charge transport normal to the layers because the charge carriers can
6   move through the minibands; the narrower the barrier, the wider the mini-
7   band and the higher the carrier mobility. Normal transport in MQW structures
8   (thick barriers) require thermionic emission of carriers over the barriers, or
9   if electric fields are applied, field-assisted tunneling through the barriers [34].
10
11   *2.1.1. Measurements of Hot Electron Cooling Dynamics in QWs and*
12   *Superlattices*
13   Hot-electron cooling times can be determined from several types of
14   time-resolved PL experiments. One technique involves hot luminescence
15   non-linear correlation [35–37], which is a symmetrized pump-probe type of
16   experiment. Fig. 2 of Ref. [35] compares the hot-electron relaxation times
17   as a function of the electron energy level in the well for bulk GaAs and a
18   20-period MQW of GaAs/$Al_{0.38}Ga_{0.62}As$ containing 250 Å GaAs wells and
19   250 Å $Al_{0.38}Ga_{0.62}As$ barriers. For bulk GaAs, the hot-electron relaxation
20   time varies from about 5 ps near the top of the well to 35 ps near the bottom
21   of the well. For the MQW, the corresponding hot-electron relaxation times
22   are 40 ps and 350 ps.
23   Another method uses time-correlated single-photon counting to meas-
24   ure PL lifetimes of hot electrons. Fig. 4 shows 3-D plots of PL intensity as a
25   function of energy and time for bulk GaAs and a 250 Å/250 Å GaAs/
26   $Al_{0.38}Ga_{0.62}As$ MQW [20]. It is clear from these plots that the MQW sample
27   exhibits much longer-lived hot luminescence (i.e., luminescence above the
28   lowest $n = 1$ electron to heavy-hole transition at 1.565 eV) than bulk GaAs.
29   Depending upon the emitted photon energy, the hot PL for the MQW is seen
30   to exist beyond times ranging from hundreds to several thousand ps. On the
31   other hand, the hot PL intensity above the bandgap (1.514 eV) for bulk
32   GaAs is negligible over most of the plot; it is only seen at the very earliest
33   times and at relatively low photon energies.
34   Calculations were performed [20] on the PL intensity versus time and
35   energy data to determine the time dependence of the quasi-Fermi-level, elec-
36   tron temperature, electronic specific heat, and ultimately the dependence of the
37   characteristic hot-electron cooling time on electron temperature.
38   The cooling, or energy-loss, rate for hot electrons is determined by
39   LO phonon emission through electron–LO–phonon interactions. The time
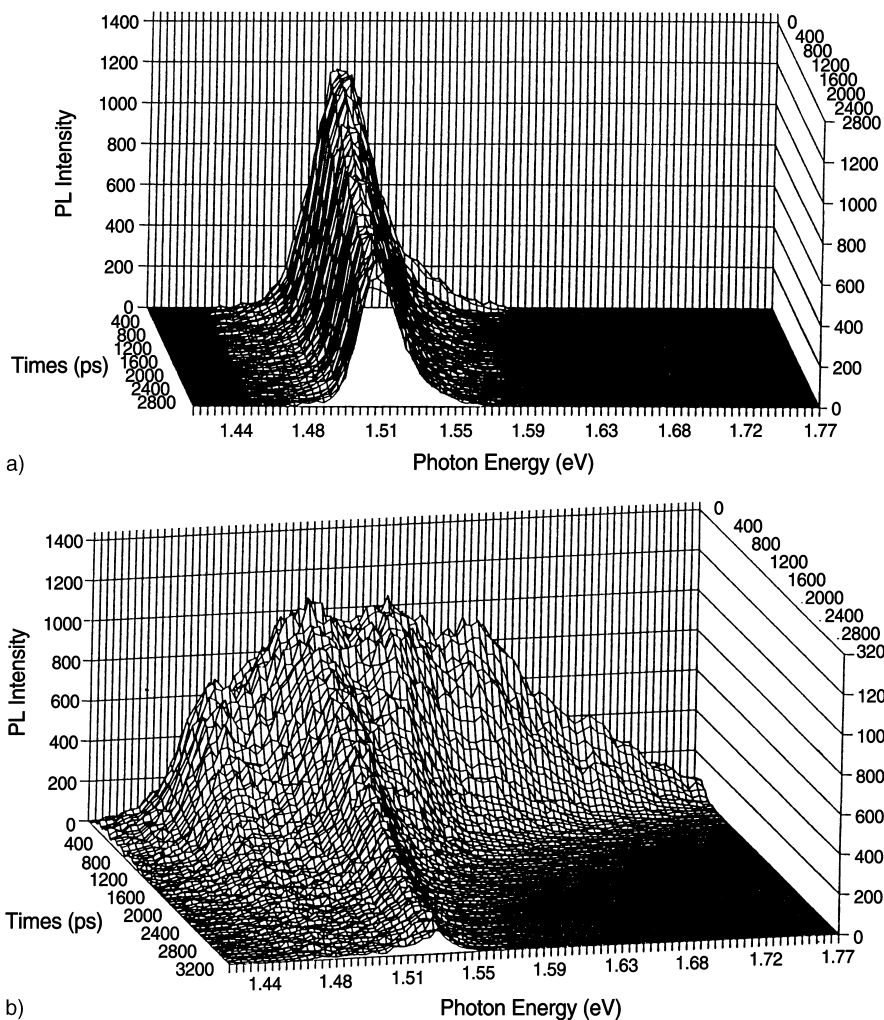
Fig. 4. Three-dimensional plots of PL intensity versus time and photon energy for (A) bulk GaAs and (B) 250 Å GaAs/250 Å Al$_{0.38}$Ga$_{0.62}$As MQW.

constant characterizing this process can be described by the following expression [38–40]:

$$P_e = -\frac{dE}{dt} = \frac{\hbar\omega_{LO}}{\tau_{avg}} \exp(-\hbar\omega_{LO}/kT_e) \tag{3}$$

1 where P_e is the power loss of electrons (i.e., the energy-loss rate), hT_{LO} the LO
2 phonon energy (36 meV in GaAs), T_e the electron temperature, and τ_{avg} the
3 time constant characterizing the energy-loss rate.
4   The electron energy-loss rate is related to the electron temperature decay
5 rate through the electronic specific heat. Since at high light intensity the elec-
6 tron distribution becomes degenerate, the classical specific heat is no longer
7 valid. Hence, the temperature and density-dependent specific heat for both
8 the QW and bulk samples need to be calculated as a function of time in each
9 experiment so that τ_{avg} can be determined.
10   The results of such calculations (presented in Fig. 2 of Reference [20])
11 show a plot of τ_{avg} versus electron temperature for bulk and MQW GaAs at
12 high and low carrier densities. These results show that at a high carrier den-
13 sity [$n \sim (2\text{–}4) \times 10^{18}\,\text{cm}^{-3}$], the τ_{avg} values for the MQW are much higher
14 ($\tau_{avg} = 350\text{–}550$ ps for T_e between 440 and 400 K) compared to bulk GaAs
15 ($\tau_{avg} = 10\text{–}15$ ps over the same T_e interval). On the other hand, at a low carrier
16 density [$n \sim (3\text{–}5) \times 10^{17}\,\text{cm}^{-3}$] the differences between the τ_{avg} values for
17 bulk and MQW GaAs are much smaller.
18   A third technique to measure cooling dynamics is PL upconversion [20].
19 Time resolved luminescence spectra were recorded at room temperature for
20 a 4000 Å bulk GaAs sample at the incident pump powers of 25, 12.5, and
21 5 mW. The electron temperatures were determined by fitting the high-energy
22 tails of the spectra; only the region which is linear on a semilogarithmic plot
23 was chosen for the fit. The carrier densities for the sample were 1×10^{19},
24 5×10^{18}, and $2 \times 10^{18}\,\text{cm}^{-3}$, corresponding to the incident excitation powers
25 of 25, 12.5, and 5 mV, respectively. Similarly, spectra for the MQW sample
26 were recorded at the same pump powers as the bulk. Fig. 5 shows τ_{avg} for bulk
27 and MQW GaAs at the 3 light intensities, again showing the much slower
28 cooling in MQWs (by up to two orders of magnitude).
29   The difference in hot-electron relaxation rates between bulk and quan-
30 tized GaAs structures is also reflected in time-integrated PL spectra. Typical
31 results are shown in Fig. 6 for single photon counting data taken with 13
32 spec pulses of 600 nm light at 800 kHz focused to about 100 μm with an
33 average power of 25 mW [41]. The time-averaged electron temperatures
34 obtained from fitting the tails of these PL spectra to the Boltzmann function
35 show that the electron temperature varies from 860 K for the 250 Å/250 Å
36 MQW to 650 K for the 250 Å/17 Å superlattice, while bulk GaAs has an
37 electron temperature of 94 K, which is close to the lattice temperature
38 (77 K). The variation in the electron temperatures between the quantized
39 structures can be attributed to differences in electron delocalization between
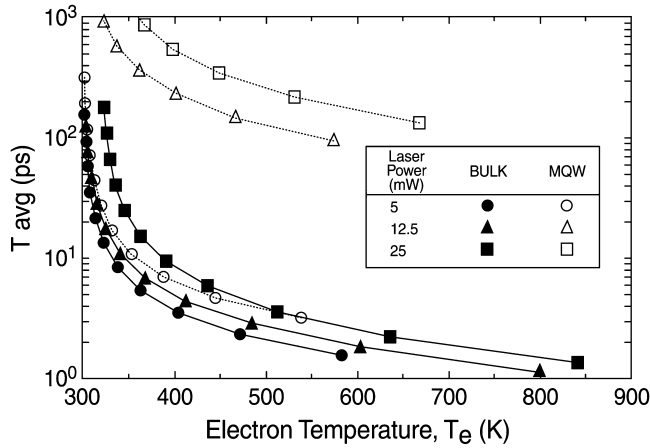
Fig. 5. Time constant for hot-electron cooling (τ_{avg}) vs electron temperature for bulk GaAs and GaAs MQWs at three excitation intensities.

MQWs and SLs, and the associated non-radiative quenching of hot-electron emission.

As shown above, the hot carrier cooling rates depend upon photogenerated carrier density; the higher the electron density the slower the cooling rate. This effect is also found for bulk GaAs, but it is much weaker compared to quantized GaAs. The most generally accepted mechanism for the decreased cooling rates in GaAs QWs is an enhanced "hot phonon bottleneck" [42–44]. In this mechanism a large population of hot carriers produces a non-equilibrium distribution of phonons (in particular, optical phonons which are the type involved in the electron–phonon interactions at high carrier energies) because the optical phonons cannot equilibrate fast enough with the crystal bath; these hot phonons can be re-absorbed by the electron plasma to keep it hot. In QWs the phonons are confined in the well and they exhibit slab modes [43], which enhance the "hot phonon bottleneck" effect.

An investigation of PV cells that are based on a p–i–n structure with the i-region consisting of a superlattice has been reported [45]. The concept is to use a superlattice region with a low value of the lowest energy transition to absorb a large fraction of the solar photons, create a hot-electron distribution within the superlattice layer that cools slowly because of the miniband formation, separate the hot electrons and holes and transport them to the higher bandgap n- and p-contacts using the electric field produced by the p–i–n structure. The results show that the concept for higher efficiency hot carrier
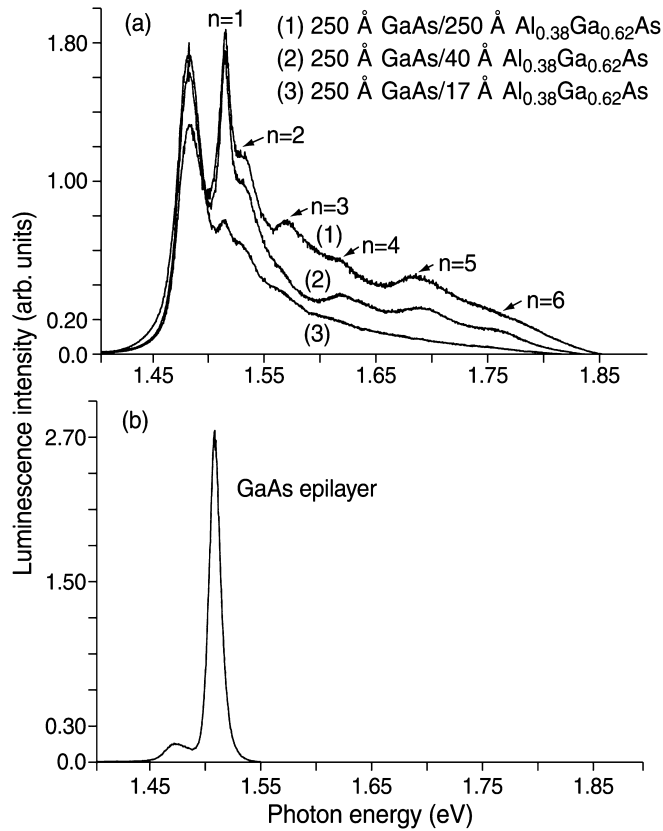
Fig. 6. (a) Time-integrated PL spectra for MQWs and SLs showing hot luminescence tails and high-energy peaks arising from hot-electron radiative recombination form upper quantum levels. (b) Equivalent spectrum for bulk GaAs showing no hot luminescence.

production and transport is undermined by the fact that under operating conditions of forward bias for the cell, cold carriers from the contacts are injected in the superlattice region and lower the hot carrier temperature. This effect could perhaps be alleviated by using selective contacts; the use of solar concentration may also help to improve conversion efficiency.

2.2. Relaxation Dynamics of Hot Excitons in Quantum Dots

As discussed above, slowed hot-electron cooling in QWs and superlattices that is produced by a *hot* phonon bottleneck requires very high light intensities in order to create the required photogenerated carrier density of greater than about $1 \times 10^{18}\,\text{cm}^{-3}$. This required intensity, possible with laser

1   excitation, is many orders of magnitude greater than that provided by solar
2   radiation at the earth's surface (maximum solar photon flux is about
3    $10^{18}\,\mathrm{cm}^{-2}\,\mathrm{s}^{-1}$; assuming a carrier lifetime of 1 ns and an absorption coefficient
4   of $1 \times 10^5\,\mathrm{cm}^{-1}$, this translates into a photoinduced electron density of about
5    $10^{14}\,\mathrm{cm}^{-3}$ at steady state). Hence, it is not possible to obtain slowed hot carrier
6   cooling in semiconductor QWs and superlattices with solar irradiation via a
7   *hot* phonon bottleneck effect; solar concentration ratios greater than 10^4
8   would be required, resulting in severe practical problems.
9   However, the situation with three-dimensional confinement in QDs is
10   potentially more favorable. In the QD case, slowed hot-electron cooling is the-
11   oretically possible even at arbitrarily low light intensity; this effect is simply
12   called a "phonon bottleneck," without the qualification of requiring hot
13   phonons (i.e., a non-equilibrium distribution of phonons). Furthermore, it is
14   also anticipated that the slowed cooling could make the rate of exciton multi-
15   plication (inverse Auger effect) an important process in QDs [1, 13, 46, 47]. PL
16   blinking in QDs (intermittent PL as a function of time) has been explained
17   [48, 49] by an Auger process whereby if two electron–holes pairs are photo-
18   generated in a QD, one pair recombines and transfers its recombination energy
19   to one of the remaining charge carriers, ionizing it over the potential barrier at
20   the surface into the surface region. This creates a charged QD that quenches
21   radiative emission after subsequent photon absorption; after some time, the
22   ionized electron can return to the QD core and the PL is turned on again. Since
23   this Auger process can occur in QDs, the inverse Auger process, whereby one
24   high-energy electron–hole pair (created from a photon with $h\nu > \mathrm{E_g}$) can
25   generate two electron–hole pairs, can also occur in QDs [47]. The following
26   discussion will present a discussion of the hot carrier cooling dynamics.
27
28   *2.2.1. Phonon Bottleneck and Slowed Hot-Electron*
29   *Cooling in Quantum Dots*
30   The first prediction of slowed cooling at low light intensities in quan-
31   tized structures was made by Boudreaux, Williams and Nozik [3]. They antic-
32   ipated that cooling of carriers would require multi-phonon processes when the
33   quantized levels are separated in energy by more than phonon energies. They
34   analyzed the expected slowed cooling time for hot holes at the surface of
35   highly-doped n-type TiO_2 semiconductors, where quantized energy levels
36   arise because of the narrow space charge layer (i.e., depletion layer) produced
37   by the high doping level. The carrier confinement in this case is produced by
38   the band bending at the surface; for a doping level of $1 \times 10^{19}\,\mathrm{cm}^{-3}$ the
39   potential well can be approximated as a triangular well extending 200 Å from

the semiconductor bulk to the surface and with a depth of 1 eV at the surface barrier. The multiphonon relaxation time was estimated from

$$\vartheta_c \sim T^{-1} \exp(E/kT) \tag{4}$$

where ϑ_c is the hot carrier cooling time, T is the phonon frequency, and E is the energy separation between quantized levels. For strongly quantized electron levels, with $E > 0.2$ eV, ϑ_c could be >100 ps according to Equation (4).

However, carriers in the space charge layer at the surface of a heavily doped semiconductor are only confined in one dimension, as in a quantum film. This quantization regime leads to discrete energy states which have dispersion in k-space [50]. This means the hot carriers can cool by undergoing inter-state transitions that require only one emitted phonon followed by a cascade of single phonon intrastate transitions; the bottom of each quantum state is reached by intrastate relaxation before an interstate transition occurs. Thus, the simultaneous and slow multiphonon relaxation pathway can be bypassed by single phonon events, and the cooling rate increases correspondingly.

More complete theoretical models for slowed cooling in QDs have been proposed by Bockelmann and co-workers [23, 51] and Benisty and co-workers [22, 24]. The proposed Benisty mechanism [22, 24] for slowed hot carrier cooling and phonon bottleneck in QDs requires that cooling only occurs via LO phonon emission. However, there are several other mechanisms by which hot electrons can cool in QDs. Most prominent among these is the Auger mechanism [52]. Here, the excess energy of the electron is transferred via an Auger process to the hole, which then cools rapidly because of its larger effective mass and smaller energy level spacing. Thus, an Auger mechanism for hot-electron cooling can break the phonon bottleneck [52]. Other possible mechanisms for breaking the phonon bottleneck include electron–hole scattering [53], deep level trapping [54], and acoustical–optical phonon interactions [55, 56].

2.2.2. *Experimental Determination of Relaxation/Cooling Dynamics and a Phonon Bottleneck in Quantum Dots*

Over the past several years, many investigations have been published that explore hot-electron cooling/relaxation dynamics in QDs and the issue of a phonon bottleneck in QDs. The results are controversial, and there are many reports that both support [25–27, 57–74] and contradict [27, 54, 75–88] the prediction of slowed hot-electron cooling in QDs and the existence of

1 a phonon bottleneck. One element of confusion that is specific to the focus of
2 this manuscript is that while some of these publications report relatively long
3 hot-electron relaxation times (tens of ps) compared to what is observed in bulk
4 semiconductors, the results are reported as being not indicative of a phonon
5 bottleneck because the relaxation times are not excessively long and PL is
6 observed [89–91] (theory predicts very long relaxation lifetimes (hundreds
7 of ns to μs) of excited carriers for the extreme, limiting condition of a full
8 phonon bottleneck; thus, the carrier lifetime would be determined by non-
9 radiative processes and PL would be absent). However, since the interest here
10 is on the rate of relaxation/cooling compared to the rate of electron separa-
11 tion and transfer, and MEG, we consider that slowed relaxation/cooling of
12 carriers has occurred in QDs if the relaxation/cooling times are greater than
13 3–5 ps (about an order of magnitude greater than that for bulk semiconductors).
14 This is because electron separation and transport and MEG can be very fast
15 (sub-ps). For solar fuel production, previous work that measured the time of
16 electron transfer from bulk III–V semiconductors to redox molecules (met-
17 allocenium cations) adsorbed on the surface found that ET times can also be
18 sub-ps to several ps [92–95]; hence photoinduced hot carrier separation,
19 transport, and transfer can be competitive with electron cooling and relaxation
20 if the latter is greater than about 10 ps. MEG rates can also be in the sub-ps
21 regime [5, 96].

22 In a series of papers, Sugawara et al. [62, 63, 65] have reported slow
23 hot-electron cooling in self-assembled InGaAs QDs produced by Stranski-
24 Krastinow (SK) growth on lattice-mismatched GaAs substrates. Using time-
25 resolved PL measurements, the excitation-power dependence of PL, and the
26 current dependence of electroluminescence spectra, these researchers report
27 cooling times ranging from 10 ps to 1 ns. The relaxation time increased with
28 electron energy up to the 5th electronic state. Also, Mukai and Sugawara [97]
29 have recently published an extensive review of phonon bottleneck effects
30 in QDs, which concludes that the phonon bottleneck effect is indeed present
31 in QDs.

32 Gfroerer et al. report slowed cooling of up to 1 ns in strain-induced GaAs
33 QDs formed by depositing tungsten stressor islands on a GaAs QW with
34 AlGaAs barriers [74]. A magnetic field was applied in these experiments to
35 sharpen and further separate the PL peaks from the excited state transitions,
36 and thereby determine the dependence of the relaxation time on level separa-
37 tion. The authors observed hot PL from excited states in the QD, which could
38 only be attributed to slow relaxation of excited (i.e., hot) electrons. Since the
39 radiative recombination time is about 2 ns, the hot-electron relaxation time

1   was found to be of the same order of magnitude (about 1 ns). With higher
2   excitation intensity sufficient to produce more than one electron–hole pair per
3   dot the relaxation rate increased.
4   A lifetime of 500 ps for excited electronic states in self-assembled InAs/
5   GaAs QDs under conditions of high injection was reported by Yu et al. [69].
6   PL from a single GaAs/AlGaAs QD [72] showed intense high-energy PL
7   transitions, which were attributed to slowed electron relaxation in this QD
8   system. Kamath et al. [73] also reported slow electron cooling in InAs/
9   GaAs QDs.
10   QDs produced by applying a magnetic field along the growth direction
11   of a doped InAs/AlSb QW showed a reduction in the electron relaxation
12   rate from $10^{12}\,s^{-1}$ to $10^{10}\,s^{-1}$ [64, 98].
13   In addition to slow electron cooling, slow hole cooling was reported by
14   Adler et al. [70, 71] in SK InAs/GaAs QDs. The hole relaxation time was
15   determined to be 400 ps based on PL rise times, while the electron relaxation
16   time was estimated to be less than 50 ps. These QDs only contained one elec-
17   tron state, but several hole states; this explained the faster electron cooling time
18   since a quantized transition from a higher quantized electron state to the
19   ground electron state was not present. Heitz et al. [66] also report relaxation
20   times for holes of about 40 ps for stacked layers of SK InAs QDs deposited
21   on GaAs; the InAs QDs are overgrown with GaAs and the QDs in each layer
22   self-assemble into an ordered column. Carrier cooling in this system is about
23   two orders of magnitude slower than in higher-dimensional structures.
24   All of the above studies on slowed carrier cooling were conducted on
25   self-assembled SK type of QDs. Studies of carrier cooling and relaxation
26   have also been performed on II–VI CdSe colloidal QDs by Klimov et al. [57,
27   81], Guyot-Sionnest et al. [60], Ellingson et al. [26], and Blackburn et al.
28   [25]. The Klimov group first studied electron relaxation dynamics from the
29   first-excited 1P to the ground 1S state using interband pump-probe spec-
30   troscopy [81]. The CdSe QDs were pumped with 100 fs pulses at 3.1 eV to
31   create high-energy electron and holes in their respective band states, and
32   then probed with fs white light continuum pulses. The dynamics of the
33   interband bleaching and induced absorption caused by state filling was
34   monitored to determine the electron relaxation time from the 1P to the 1S
35   state. The results showed very fast 1P to 1S relaxation, on the order of
36   300 fs, and were attributed to an Auger process for electron relaxation which
37   bypassed the phonon bottleneck. However, this experiment cannot separate
38   the electron and hole dynamics from each other. Guyot-Sionnest et al. [60]
39   followed up these experiments using fs infrared pump-probe spectroscopy.

1   A visible pump beam creates electrons and holes in the respective band states
2   and a subsequent IR beam is split into an IR pump and an IR probe beam;
3   the IR beams can be tuned to monitor only the intraband transitions of the
4   electrons in the electron states, and thus can separate electron dynamics from
5   hole dynamics. The experiments were conducted with CdSe QDs that were
6   coated with different capping molecules (TOPO, thiocresol, and pyridine),
7   which exhibit different hole-trapping kinetics. The rate of hole trapping
8   increased in the order: TOPO, thiocresol, and pyridine. The results generally
9   show a fast relaxation component (1–2 ps) and a slow relaxation component
10 ($\approx$200 ps). The relaxation times follow the hole-trapping ability of the differ-
11 ent capping molecules, and are longest for the QD systems having the fastest
12 hole-trapping caps; the slow component dominates the data for the pyridine
13 cap, which is attributed to its faster hole-trapping kinetics.
14   These results [60] support the Auger mechanism for electron relaxation,
15 whereby the excess electron energy is rapidly transferred to the hole which
16 then relaxes rapidly through its dense spectrum of states. When the hole is
17 rapidly removed and trapped at the QD surface, the Auger mechanism for hot-
18 electron relaxation is inhibited and the relaxation time increases. Thus, in the
19 above experiments, the slow 200 ps component is attributed to the phonon
20 bottleneck, most prominent in pyridine-capped CdSe QDs, while the fast
21 1–2 ps component reflects the Auger relaxation process. The relative weight of
22 these two processes in a given QD system depends upon the hole-trapping
23 dynamics of the molecules surrounding the QD.
24   Klimov et al. further studied carrier relaxation dynamics in CdSe QDs
25 and published a series of papers on the results [57, 58]; a review of this work
26 was also recently published [59]. These studies also strongly support the pres-
27 ence of the Auger mechanism for carrier relaxation in QDs. The experiments
28 were done using ultrafast pump-probe spectroscopy with either 2 beams or
29 3 beams. In the former, the QDs were pumped with visible light across its
30 bandgap (hole states to electron states) to produce excited state (i.e., hot)
31 electrons; the electron relaxation was monitored by probing the bleaching
32 dynamics of the resonant HOMO to LUMO transition with visible light, or by
33 probing the transient IR absorption of the 1S to 1P intraband transition, which
34 reflects the dynamics of electron occupancy in the LUMO state of the QD.
35 The 3 beam experiment was similar to that of Guyot-Sionnest et al. [60]
36 except that the probe in the experiments of Klimov et al. is a white light con-
37 tinuum. The first pump beam is at 3 eV and creates electrons and holes across
38 the QD bandgap. The second beam is in the IR and is delayed with respect to
39 the optical pump; this beam re-pumps electrons that have relaxed to the

1   LUMO backup in energy. Finally, the third beam is a broad band white light
2   continuum probe that monitors photoinduced interband absorption changes
3   over the range of 1.2 to 3 eV. The experiments were done with two different
4   caps on the QDs: a ZnS cap and a pyridine cap. The results showed that with
5   the ZnS-capped CdSe the relaxation time from the 1P to 1S state was about
6   250 fs, while for the pyridine-capped CdSe, the relaxation time increased to
7   3 ps. The increase in the latter experiment was attributed to a phonon bottle-
8   neck produced by rapid hole trapping by the pyridine, as also proposed by
9   Guyot-Sionnest et al. [60]. However, the time scale of the phonon bottleneck
10   induced by hole trapping by pyridine caps on CdSe that were reported by
11   Klimov et al. was not as great as that reported by Guyot-Sionnest et al. [60].
12   Recent results were reported [25, 26] for the electron cooling dynamics
13   in InP QDs where the QD surface was modified to affect hole trapping and also
14   where only electrons were injected into the QD from an external redox mole-
15   cule (sodium biphenyl) so that holes necessary for the Auger cooling mecha-
16   nism were not present in the QD [25]. For InP, HF etching was found to
17   passivate electronic surface states but not hole surface states [99, 100]; thus
18   holes can become localized at the surface in both etched and unetched TOPO-
19   capped QDs, and the dynamics associated with these two samples will not
20   deviate significantly. The relaxation was found to be bi-exponential and sug-
21   gests the presence of two subsets of QDs within the sample [25, 26]. Since
22   etching has been shown to inefficiently passivate hole traps, it is proposed
23   that two subsets of QDs are probed in the experiment: one subset in which the
24   hole and electron are efficiently confined to the interior of the nanocrystal
25   (hole trap absent; exciton confined to the QD core), and one subset in which
26   the hole is localized at the surface of the QD on a phosphorous dangling bond
27   (hole trap present; charge-separated QD) [25, 26].
28   With the electron and hole confined to the QD core, strong electron–hole
29   interaction leads to efficient, fast relaxation via the Auger mechanism, and in
30   QDs where the hole is localized at the surface the increased spatial separation
31   inhibits the Auger process and results in slower relaxation. The data imply
32   that hole trapping at the intrinsic surface state occurs in less than 75 fs [25].
33   To further investigate the mechanisms involved in the intraband relax-
34   ation, experiments were conducted in which only electrons are present in the
35   QDs and holes are absent. Sodium biphenyl is a very strong reducing agent
36   which has been shown to successfully inject electrons into the conduction band
37   of CdSe QDs [101, 102], effectively bleaching the 1S transition and allowing
38   an IR-induced transition to the $1P_e$ level. Sodium biphenyl was therefore
39   used to inject electrons into the 1S electron level in InP QDs [25]. This $1S_e$
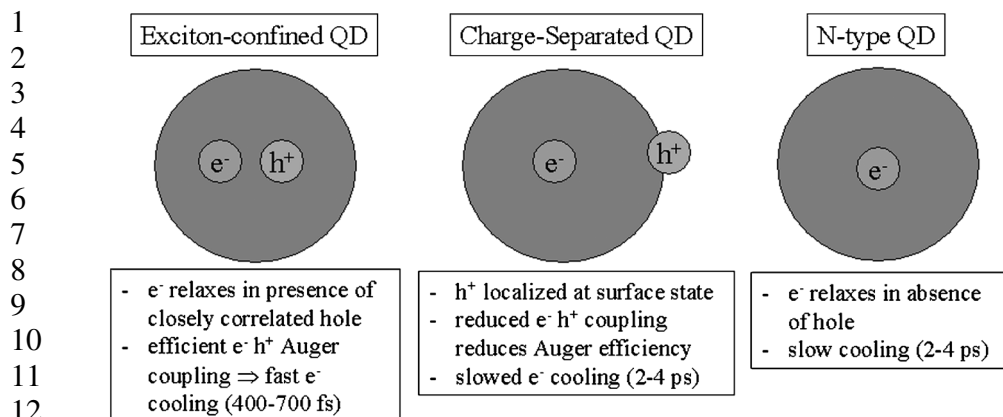
Fig. 7. Different electron–hole configurations in a QD and the resulting relaxation/cooling dynamics.

electron may be excited to the $1P_e$ level with an IR pump and its relaxation dynamics back to the ground 1S state monitored. Time-resolved, IR-induced transitions in n-type (electron injected) InP QDs show that the relaxation of the excited electrons from the 1P to the 1S level can be fit to a single exponential, with an average time constant of 3.0 ps, corresponding to a relaxation rate of 0.092 eV ps^{-1}; in neutral 50 Å TOP/TOPO-capped InP QDs, the relaxation shows a large 400 fs component indicative of fast electron cooling. Similar conclusions were reported for electrons injected into ZnO and CdSe colloidal QDs [27]. These experiments confirm that in the absence of a core-confined hole, electronic relaxation is slowed by about an order of magnitude. However, it should be noted that the relaxation rate in the absence of a hole is close to the relaxation rate with the hole localized at the surface. This is surprising and raises the question of why electron cooling in the absence of a hole is not longer. Possible explanations have been proposed [103] including that (1) positive counter ions of the oxidized sodium biphenyl are adsorbed on the QD surface and behave like a trapped hole in producing a significant Coulomb interaction with the electron to permit Auger cooling and (2) an enhanced Huang-Rhees parameter occurs in charged QDs and enhances multi-phonon relaxation. A summary of these experiments investigating the effects of elec-tron cooling on electron–hole separation is shown in Fig. 7.

Recent results by Guyot-Sionnest et al. show that the nature of the sur-face ligands has a major effect on the relaxation dynamics [27]. Depend-ing upon the surface ligand stabilizing the QDs, the relaxation or cooling

1   dynamics of hot excitons could be varied from 3.8 ps for tetradecylphosphonic
2   acid, 8 ps for oleic acid, 10 ps for octadecylamine, to 27 ps for dodecanethiol
3   ligands. The later cooling rate is nearly 2 orders of magnitude slower than that
4   for naked QDs or QDs capped with TOP-TOPO.

5   In contradiction to the results showing slowed cooling in QDs, many
6   other investigations exist in the literature in which a phonon bottleneck was
7   apparently not observed. These results were reported for both self-organized
8   SK QDs [54, 75–88] and II–VI colloidal QDs [81, 83, 85]. However, in sev-
9   eral cases [66, 89, 91], hot-electron relaxation was found to be slowed, but
10 not sufficiently for the authors to conclude that this was evidence of a
11 phonon bottleneck.

13 ## 3. MULTIPLE EXCITON GENERATION IN QUANTUM DOTS

15 The formation of multiple electron–hole pairs per absorbed photon in photo-
16 excited bulk semiconductors is a process typically explained by impact ioniza-
17 tion (I.I.). In this process, an electron or hole with kinetic energy greater than
18 the semiconductor bandgap produces one or more additional electron–hole
19 pairs. The kinetic energy can be created either by applying an electric field or
20 by absorbing a photon with energy above the semiconductor bandgap energy.
21 The former is well studied and understood [104–106]. The latter process is
22 less well studied, but has been observed in photoexcited p–n junctions of Si,
23 Ge, and InSb [107–110].

24   However, impact ionization has not contributed meaningfully to
25 improved quantum yield in working solar cells, primarily because the I.I. effi-
26 ciency does not reach significant values until photon energies reach the ultra-
27 violet region of the spectrum. In bulk semiconductors, the threshold photon
28 energy for I.I. exceeds that required for energy conservation alone because, in
29 addition to conserving energy, crystal momentum must be conserved. Addi-
30 tionally, the rate of I.I. must compete with the rate of energy relaxation by
31 electron–phonon scattering. It has been shown that the rate of I.I. becomes
32 competitive with phonon scattering rates only when the kinetic energy of the
33 electron is many times the bandgap energy (E_g) [104–106]. The observed
34 transition between inefficient and efficient I.I. occurs slowly; for example,
35 in Si the I.I. efficiency was found to be only 5% (*i.e.*, total quantum
36 yield = 105%) at $h\nu \approx 4\,\text{eV}(3.6E_g)$, and 25% at $h\nu \approx 4.8\,\text{eV}$ $(4.4E_g)$ [110,
37 111]. This large blue-shift of the threshold photon energy for I.I. in semicon-
38 ductors prevents materials such as bulk Si and GaAs from yielding
39 improved solar conversion efficiencies [11, 111].

1   However, in QDs the rate of electron relaxation through electron–phonon
2 interactions can be significantly reduced because of the discrete character of
3 the electron–hole spectra, and the rate of Auger processes, including the
4 inverse Auger process of exciton multiplication, is greatly enhanced due to
5 carrier confinement and the concomitantly increased electron–hole Coulomb
6 interaction. Furthermore, crystal momentum need not be conserved because
7 momentum is not a good quantum number for three-dimensionally-confined
8 carriers. Indeed, very efficient multiple electron–hole pair (multi-exciton)
9 creation by one photon was reported recently in PbSe nanocrystals by
10 Schaller and Klimov [14]. They reported an excitation energy threshold for
11 the formation of two excitons per photon at $3E_g$, where E_g is the absorption
12 energy gap of the nanocrystal (HOMO-LUMO transition energy. Schaller
13 and Klimov reported a QY value of 218% (118% I.I. efficiency) at $3.8E_g$;
14 QYs above 200% indicate the formation of more than two excitons per
15 absorbed photon. Other researchers have recently reported [5] a QY value
16 of 300% for 3.9 nm diameter PbSe QDs at a photon energy of $4E_g$, indicat-
17 ing the formation of three excitons per photon for every photoexcited QD in
18 the sample. Evidence was also provided that showed the threshold for MEG
19 by optical excitation is $2E_g$, not $3E_g$ as reported previously for PbSe QDs
20 [14], and it was also shown that comparably efficient MEG occurs also in
21 PbS nanocrystals. A new possible mechanism for MEG was introduced [14]
22 that invokes a coherent superposition of multiple-excitonic states, meaning
23 that multiple excitons are essentially created instantly upon absorption of
24 high-energy photons. Most recently, MEG has been reported in CdSe QDs
25 [112], and in PbTe QDs [113] and seven excitons per photon were reported
26 in PbSe QDs at 7 times the bandgap [112].

27   Multiexcitons are detected by monitoring the signature of multiexciton
28 decay dynamics using transient absorption (TA) spectroscopy [5, 14, 112].
29 The magnitude of the photoinduced absorption change at the band edge is
30 proportional to the number of electron–hole pairs created in the sample. The
31 transients are detected by probing either with a band edge (energy gap or
32 HOMO-LUMO transition energy $\equiv E_g$) probe pulse, or with a mid-IR probe
33 pulse that monitors intraband transitions in the newly created excitons.
34 Although both the band-edge and mid-IR probe signals would incorporate
35 components from excitons with energy above the $1S_h$–$1S_e$ exciton, multiple-
36 exciton Auger recombination analysis relies only on data for delays >5 ps,
37 by which time carrier multiplication and cooling are complete.

38   The dependence of the MEG QY on the ratio of the pump photon energy
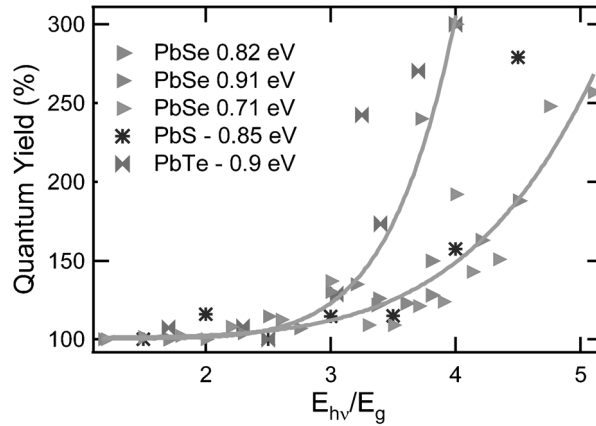39 to the bandgap ($E_{h\nu}/E_g$) is shown in Fig. 8 for PbSe, PbS, and PbTe QDs.

Fig. 8. MEG QYs for PbS, PbSe, PbTe, the solid lines are guides to the eye.

For the 3 PbSe QD samples, E_g = 0.72 eV (dia. = 5.7 nm), E_g = 0.82 eV (dia. = 4.7 nm), and E_g = 0.91 eV (dia. = 3.9 nm). For all three samples, the sharp rise in QY begins at about three times the energy gap, a result in agreement with that reported. The data show that for the 3.9 nm QD (E_g = 0.91 eV), the QY reaches a value of 300% at $E_{h\nu}/E_g$ = 4.0, indicating that the QDs produce three excitons per absorbed photon. For the other two PbSe samples (E_g = 0.82 eV (4.7 nm dia.) and 0.72 eV (5.7 nm dia.)), it is estimated that a QY of 300% is reached at an $E_{h\nu}/E_g$ value of 5.5. It was noted that the $2P_h$–$2P_e$ transition in the QDs is resonant with the $3E_g$ excitation, corresponding to the sharp onset of increased MEG efficiency. If this symmetric transition ($2P_h$–$2P_e$) dominates the absorption at ~ $3E_g$, the resulting excited state provides both the electron and the hole with excess energy of $1E_g$, in resonance with the lowest exciton absorption (at $1E_g$). Our data also showed that the QY begins to surpass 100% at E_h/E_g values greater than 2.0 (see Fig. 3). In ref. [5], 16 QY values were carefully measured between $2.1E_g$ and $2.9E_g$ (mean value = 109.8%) and 11 QY values between $1.2E_g$ and $2.0E_g$ (mean value = 101.3%). Application of statistical t-tests show that the QY values for photon energies between $1E_g$ and $2E_g$ were not statistically different from 100% (P value = 0.105), while the difference in QYs between $1.2E_g$–$2.0E_g$ and $2.1E_g$–$2.9E_g$ were very statistically significant with a P value of 0.001. Also, simple visual inspection of Fig. 3 indicated a significant difference between the QY values between $1E_g$–$2E_g$ and $2E_g$–$3E_g$. For PbS and PbTe QDs, the bandgaps were 0.85 and 0.90 eV, respectively, corresponding to diameters of 5.5 nm and 4.2 nm.

4. QUANTUM DOT SOLAR CELL CONFIGURATIONS

The two fundamental pathways for enhancing the conversion efficiency (increased photovoltage [2, 3] or increased photocurrent [10, 11] can be accessed, in principle, in at least three different QD solar cell configurations; these configurations are shown in Fig. 9 and they are described below. However, it is emphasized that these potential high efficiency configurations are conceptual and there is no experimental evidence yet that demonstrates actual enhanced conversion efficiencies in any of these systems.

4.1. Photoelectrodes Composed of Quantum Dot Arrays

In this configuration, the QDs are formed into an ordered 3-D array with inter-QD spacing sufficiently small such that strong electronic coupling occurs and minibands are formed to allow long-range electron transport (see Fig. 9A). The system is a 3-D analog to a 1-D superlattice and the miniband structures formed therein [1] (see Fig. 3). The delocalized quantized 3-D miniband states could be expected to slow the carrier cooling and permit the transport and collection of hot carriers to produce a higher photopotential in a PV cell or in a photoelectrochemical cell where the 3-D QD array is the photoelectrode [114]. Also, MEG might be expected to occur in the QD arrays, enhancing the photocurrent (see Fig. 2). However, hot-electron transport/collection and MEG cannot occur simultaneously; they are mutually exclusive and only one of these processes can be present in a given system.

Significant progress has been made in forming 3-D arrays of both colloidal [115–117] and epitaxial [118] II–VI and III–V QDs. The former have been formed via evaporation and crystallization of colloidal QD solutions containing a uniform QD size distribution; crystallization of QD solids from broader size distributions lead to close-packed QD solids, but with a high degree of disorder. Concerning the latter, arrays of epitaxial QDs have been formed by successive epitaxial deposition of epitaxial QD layers; after the first layer of epitaxial QDs is formed, successive layers tend to form with the QDs in each layer aligned on top of each other [118, 119]. Theoretical and experimental studies of the properties of QD arrays are currently under way. Major issues are the nature of the electronic states as a function of inter-dot distance, array order vs disorder, QD orientation and shape, surface states, surface structure/passivation, and surface chemistry. Transport properties of QD arrays are also of critical importance, and they are under investigation.
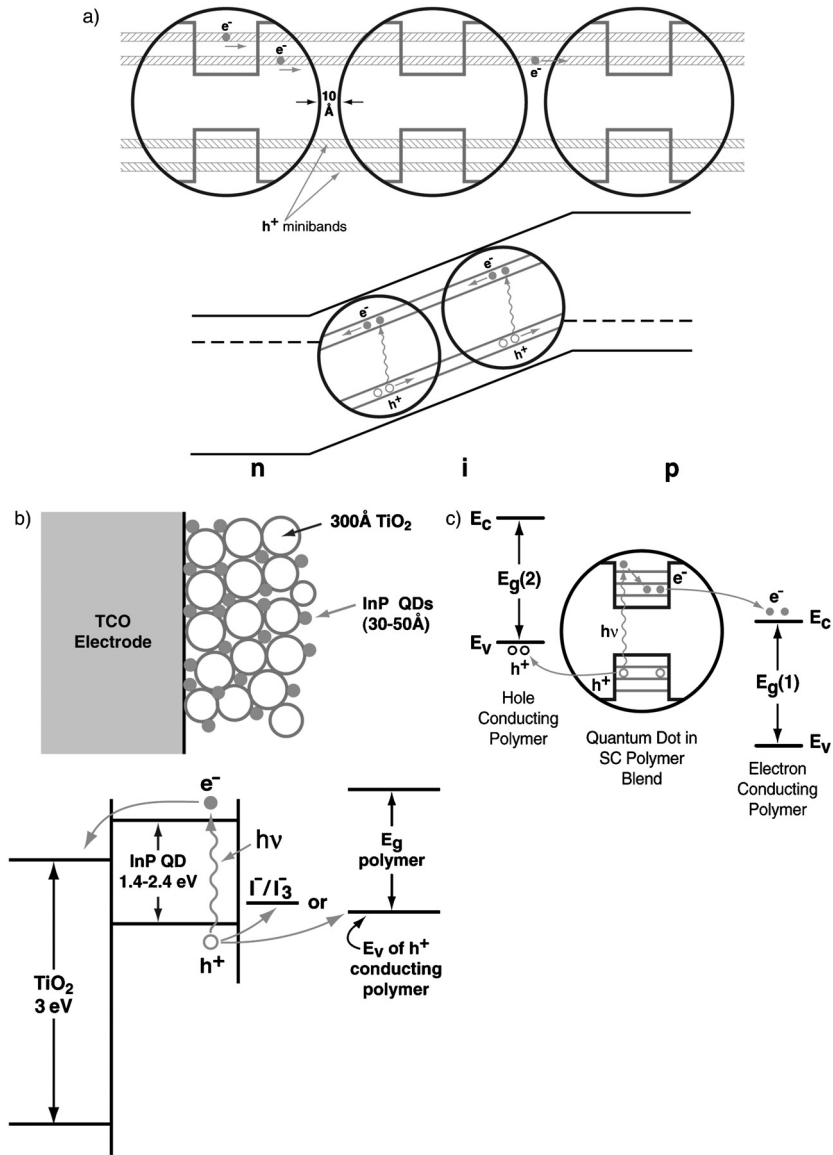
a)

b)

c)

Fig. 9. Configurations for QD solar cells. (A) a QD array used as a photoelectrode for a photoelectrochemical or as the i-region of a p–i–n PV cell; (B) QDs used to sensitize a nanocrystalline film of a wide bandgap oxide semiconductor (viz. TiO_2) to visible light. This configuration is analogous to the dye-sensitized solar cell where the dye is replaced by QDs; (C) QDs dispersed in a blend of electron- and hole-conducting polymers. In configurations A, B, C, the occurrence of impact ionization could produce higher photocurrents and higher conversion efficiency. In A, enhanced efficiency could be achieved either through impact ionization or hot carrier transport through the minibands of the QD array resulting in a higher photopotential.

1 **4.2. Quantum Dot-Sensitized Nanocrystalline TiO$_2$ Solar Cells**
2   This configuration is a variation of a recent promising new type of PV cell
3 that is based on dye-sensitization of nanocrystalline TiO$_2$ layers [120–122].
4 In this latter PV cell, dye molecules are chemisorbed onto the surface of
5 10–30 nm-size TiO$_2$ particles that have been sintered into a highly porous
6 nanocrystalline 10–20 μm TiO$_2$ film. Upon photoexcitation of the dye mole-
7 cules, electrons are very efficiently injected from the excited state of the dye
8 into the conduction band of the TiO$_2$, affecting charge separation and produc-
9 ing a PV effect. The cell circuit is completed using a non-aqueous redox elec-
10 trolyte that contains I$^-$/I$_3^-$ and a Pt counter electrode to allow reduction of
11 the adsorbed photooxidized dye back to its initial non-oxidized state (via I$_3^-$
12 produced at the Pt cathode by reduction of I$^-$).
13   For the QD-sensitized cell, QDs are substituted for the dye molecules;
14 they can be adsorbed from a colloidal QD solution [123] or produced in situ
15 [124–127] (see Fig. 9B). Successful PV effects in such cells have been
16 reported for several semiconductor QDs including InP, CdSe, CdS, and PbS
17 [123–127]. Possible advantages of QDs over dye molecules are the tunabil-
18 ity of optical properties with size and better heterojunction formation with
19 solid hole conductors. Also, as discussed here, a unique potential capability
20 of the QD-sensitized solar cell is the production of quantum yields greater
21 than one by MEG (inverse Auger effect) [47]. Dye molecules cannot
22 undergo this process. Efficient inverse Auger effects in QD-sensitized solar
23 cells could produce much higher conversion efficiencies than are possible
24 with dye-sensitized solar cells.
25
26 **4.3. Quantum Dots Dispersed in Organic Semiconductor**
27 **Polymer Matrices**
28   Recently, PV effects have been reported in structures consisting of QDs
29 forming junctions with organic semiconductor polymers. In one configuration,
30 a disordered array of CdSe QDs is formed in a hole-conducting polymer—
31 MEH-PPV (poly(2-methoxy, 5-(2′-ethyl)-hexyloxy-p-phenylenevinylene)
32 [128]. Upon photoexcitation of the QDs, the photogenerated holes are injected
33 into the MEH-PPV polymer phase, and are collected via an electrical contact
34 to the polymer phase. The electrons remain in the CdSe QDs and are col-
35 lected through diffusion and percolation in the nanocrystalline phase to
36 an electrical contact to the QD network. Initial results show relatively low
37 conversion efficiencies [128, 129] but improvements have been reported
38 with rod-like CdSe QD shapes [130] embedded in poly(3-hexylthiophene)
39 (the rod-like shape enhances electron transport through the nanocrystalline

1   QD phase). In another configuration [131], a polycrystalline TiO$_2$ layer is
2   used as the electron conducting phase, and MEH-PPV is used to conduct the
3   holes; the electron and holes are injected into their respective transport
4   mediums upon photoexcitation of the QDs.

5   A variation of these configurations is to disperse the QDs into a blend
6   of electron and hole-conducting polymers (see Fig. 9C). This scheme is the
7   inverse of light emitting diode structures based on QDs [132–136]. In the PV
8   cell, each type of carrier–transporting polymer would have a selective elec-
9   trical contact to remove the respective charge carriers. A critical factor for
10 success is to prevent electron–hole recombination at the interfaces of the two
11 polymer blends; prevention of electron–hole recombination is also critical
12 for the other QD configurations mentioned above.

13   All of the possible QD-organic polymer PV cell configurations would
14 benefit greatly if the QDs can be coaxed into producing multiple electron–
15 hole pairs by the inverse Auger/MEG process [47]. This is also true for all
16 the QD solar cell systems described above. The various cell configurations
17 simply represent different modes of collecting and transporting the photo-
18 generated carriers produced in the QDs.

CONCLUSION

22 The relaxation dynamics of photoexcited electrons in semiconductor QDs
23 can be greatly modified compared to the bulk form of the semiconductor.
24 Specifically, the cooling dynamics of highly energetic (hot) electrons cre-
25 ated by absorption of supra-bandgap photons can be slowed by at least one
26 order of magnitude (4–7 ps vs 400–700 fs). This slowed cooling is caused
27 by a so-called "phonon bottleneck" when the energy spacing between quan-
28 tized levels in the QD is greater than the LO-phonon energy, thus inhibiting
29 hot-electron relaxation (cooling) by electron–phonon interactions. In order
30 to produce the slowed hot-electron cooling via the phonon bottleneck, it is
31 necessary to block an Auger process that could bypass the phonon bottle-
32 neck and allow fast electron cooling. The Auger cooling process involves
33 the transfer of the excess electron energy to a hole, which then cools rapidly
34 because of its higher effective mass and closely-spaced energy levels.
35 Blocking the Auger cooling is achieved by rapidly removing the photogen-
36 erated hole before it undergoes Auger scattering with the photogenerated
37 electron, or by injecting electrons into the LUMO level (conduction band)
38 of the QD from an external electron donating chemical species and then
39 exciting these electrons with an IR pulse. Slowed electron cooling in QDs

1   offers the potential to use QDs in solar cells to enhance their conversion
2   efficiency. In bulk semiconductors, the hot electrons (and holes) created by
3   absorption of supra-bandgap photons cool so rapidly to the band edges that
4   the excess kinetic energy of the photogenerated carriers is converted to heat
5   and limits the theoretical Shockley-Queisser thermodynamic conversion
6   efficiency to about 32% (at one sun). Slowed cooling in QDs could lead to
7   their use in solar cell configurations wherein impact ionization (the forma-
8   tion of two or more electron–hole pairs per absorbed photon) or hot-electron
9   separation, transport, and transfer can become significant, thus producing
10 enhanced photocurrents or photovoltages and corresponding enhanced con-
11 version efficiencies with thermodynamics limits of 66% (one sun). Three
12 configurations for QD solar cells have been described here that would produce
13 either enhanced photocurrent or photovoltage.

ACKNOWLEDGMENTS

REFERENCES

[1] A.J. Nozik, Annu. Rev. Phys. Chem., 52 (2001) 193.
[2] R.T. Ross and A.J. Nozik, J. Appl. Phys., 53 (1982) 3813.
[3] D.S. Boudreaux and F. Williams, A.J. Nozik, J. Appl. Phys., 51 (1980) 2158.
[4] F.E. Williams and A.J. Nozik, Nature, 311 (1984) 21.
[5] R.J. Ellingson, M.C. Beard, J.C. Johnson, P. Yu, O.I. Micic, A.J. Nozik, A. Shabaev,
and A.L. Efros, Nano Lett., 5 (2005) 865.
[6] W. Shockley and H. J. Queisser, J. Appl. Phys., 32 (1961) 510.
[7] R.T. Ross, J. Chem. Phys., 45 (1966) 1.
[8] R.T. Ross, J. Chem. Phys., 46 (1967) 4590.
[9] R.J. Ellingson, J.L. Blackburn, P. Yu, G. Rumbles, O.I. Micic and A.J. Nozik, J. Phys.
Chem. B, 106 (2002) 7758.

*This chapter is derived from previously published reviews and manuscripts by the author in
references [1] and [13].
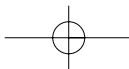
[10] P.T. Landsberg, H. Nussbaumer, G. Willeke, J. Appl. Phys., 74 (1993) 1451.

[11] S. Kolodinski, J.H. Werner, T. Wittchen, H.J. Queisser, Appl. Phys. Lett., 63 (1993) 2405.

[12] M.A. Green, Third Generation Photovoltaics, Bridge Printery, Sydney, 2001.

[13] A.J. Nozik, Physica E, 14 (2002) 115.

[14] R. Schaller, V. Klimov, Phys. Rev. Lett., 92 (2004) 186601.

[15] A. Luque, A. Marti, Phys. Rev. Lett., 78 (1997) 5014.

[16] A.J. Nozik, D.S. Boudreaux, R.R. Chance, F. Williams, Charge Transfer at Illuminated Semiconductor-Electrolyte Interfaces, in: M. Wrighton (Ed.) Advances in Chemistry, vol 184, ACS, New York, 1980, p. 162.

[17] A.J. Nozik, Philos. Trans. R. Soc. London. Ser. A, A295 (1980) 453.

[18] W.S. Pelouch, R.J. Ellingson, P.E. Powers, C.L. Tang, D.M. Szmyd, A.J. Nozik, Phys. Rev. B, 45 (1992) 1450.

[19] W.S. Pelouch, R.J. Ellingson, P.E. Powers, C.L. Tang, D.M. Szmyd, A.J. Nozik, Semicond. Sci. Technol., 7 (1992) B337.

[20] Y. Rosenwaks, M.C. Hanna, D.H. Levi, D.M. Szmyd, R.K. Ahrenkiel, A.J. Nozik, Phys. Rev. B, 48 (1993) 14675.

[21] F. Williams, A.J. Nozik, Nature, 271 (1978) 137.

[22] H. Benisty, C.M. Sotomayor-Torres, C. Weisbuch, Phys. Rev. B, 44 (1991) 10945.

[23] U. Bockelmann, G. Bastard, Phys. Rev. B, 42 (1990) 8947.

[24] H. Benisty, Phys. Rev. B, 51 (1995) 13281.

[25] J.L. Blackburn, R.J. Ellingson, O.I. Micic, A.J. Nozik, J. Phys. Chem. B, 107 (2003) 102.

[26] R.J. Ellingson, J.L. Blackburn, J.M. Nedeljkovic, G. Rumbles, M. Jones, H. Fu, A.J. Nozik, Phys. Rev. B, 67 (2003) 075308.

[27] P. Guyot-Sionnest, B. Wehrenberg, D. Yu, J. Chem. Phys., 123 (2005) 074709.

[28] J.I. Pankove, Optical Processes in Semiconductors, Dover, New York, 1975.

[29] S. Sze, Physics of Semiconductor Devices, Wiley, New York, 1981.

[30] M.A. Green, Solar Cells, The University of New South Wales, Kensington, Aust., 1992.

[31] A.J. Nozik, Annu. Rev. Phys. Chem., 29 (1978) 189.

[32] R. Dingle (Ed.) Applications of Multiquantum Wells, Selective Doping, and Superlattices, Academic Press, New York, 1987.

[33] M.W. Peterson, J.A. Turner, C.A. Parsons, A.J. Nozik, D.J. Arent, C. Van Hoof, G. Borghs, R. Houdre, H. Morkoc, Appl. Phys. Lett., 53 (1988) 2666.

[34] C.A. Parsons, B.R. Thacker, D.M. Szmyd, M.W. Peterson, W.E. McMahon, A.J. Nozik, J. Chem. Phys., 93 (1990) 7706.

[35] D.C. Edelstein, C.L. Tang, A.J. Nozik, Appl. Phys. Lett., 51 (1987) 48.

[36] Z.Y. Xu, C.L. Tang, Appl. Phys. Lett., 44 (1984) 692.

[37] M.J. Rosker, F.W. Wise, C.L. Tang, Appl. Phys. Lett., 49 (1986) 1726.

[38] J.F. Ryan, R.A. Taylor, A.J. Tuberfield, A. Maciel, J.M. Worlock, A.C. Gossard, W. Wiegmann, Phys. Rev. Lett., 53 (1984) 1841.

[39] J. Christen, D. Bimberg, Phys. Rev. B, 42 (1990) 7213.

[40] W. Cai, M.C. Marchetti, M. Lax, Phys. Rev. B, 34 (1986) 8573.

[41] A.J. Nozik, C.A. Parsons, D.J. Dunlavy, B.M. Keyes, R.K. Ahrenkiel, Solid State Comm. 75 (1990) 297.
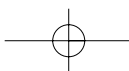
[42] P. Lugli, S.M. Goodnick, Phys. Rev. Lett., 59 (1987) 716.

[43] V.B. Campos, S. Das Sarma, M.A. Stroscio, Phys. Rev. B, 46 (1992) 3849.

[44] R.P. Joshi, D.K. Ferry, Phys. Rev. B, 39 (1989) 1180.

[45] M.C. Hanna, Z.W. Lu, A.J. Nozik, Future Generation Photovoltaic Technologies, in: R.D. McConnell (Ed.) AIP Conference Proceedings 404, American Institute of Physics, Woodbury, NY, 1997, pp. 309–317.

[46] A.J. Nozik, Next Generation Photovoltaics, in: A. Marti, M. Green (Eds.), Series in Optics and Optoelectronics, Institute of Physics, 2004, pp. 196–218.

[47] A.J. Nozik, (1997) unpublished manuscript.

[48] M. Nirmal, B.O. Dabbousi, M.G. Bawendi, J.J. Macklin, J.K. Trautman, T.D. Harris, L.E. Brus, Nature, 383 (1996) 802.

[49] A.L. Efros, M. Rosen, Phys. Rev. Lett., 78 (1997) 1110.

[50] M. Jaros, Quantum Wells, Superlattices, Quantum Wires, and Dots, in: Physics and Applications of Semiconductor Microstructures, Oxford University Press, New York, 1989, pp. 83–106.

[51] U. Bockelmann, T. Egeler, Phys. Rev. B, 46 (1992) 15574.

[52] A.L. Efros, V.A. Kharchenko, M. Rosen, Solid State Commun. 93 (1995) 281.

[53] I. Vurgaftman, J. Singh, Appl. Phys. Lett., 64 (1994) 232.

[54] P.C. Sercel, Phys. Rev. B, 51 (1995) 14532.

[55] T. Inoshita, H. Sakaki, Phys. Rev. B, 46 (1992) 7260.

[56] T. Inoshita, H. Sakaki, Phys. Rev. B, 56 (1997) R4355.

[57] V.I. Klimov, A.A. Mikhailovsky, D.W. McBranch, C.A. Leatherdale, M.G. Bawendi, Phys. Rev. B, 61 (2000) R13349.

[58] V.I. Klimov, D.W. McBranch, C.A. Leatherdale, M.G. Bawendi, Phys. Rev. B, 60 (1999) 13740.

[59] V.I. Klimov, J. Phys. Chem. B, 104 (2000) 6112.

[60] P. Guyot-Sionnest, M. Shim, C. Matranga, M. Hines, Phys. Rev. B, 60 (1999) R2181.

[61] P.D. Wang, C.M. Sotomayor-Torres, H. McLelland, S. Thoms, M. Holland, C.R. Stanley, Surf. Sci., 305 (1994) 585.

[62] K. Mukai, M. Sugawara, Jpn. J. Appl. Phys., 37 (1998) 5451.

[63] K. Mukai, N. Ohtsuka, H. Shoji, M. Sugawara, Appl. Phys. Lett., 68 (1996) 3013.

[64] B.N. Murdin, A.R. Hollingworth, M. Kamal-Saadi, R.T. Kotitschke, C.M. Ciesla, C.R. Pidgeon, P.C. Findlay, H.P.M. Pellemans, C.J.G.M. Langerak, A.C. Rowe, R.A. Stradling, E. Gornik, Phys. Rev. B, 59 (1999) R7817.

[65] M. Sugawara, K. Mukai, H. Shoji, Appl. Phys. Lett., 71 (1997) 2791.

[66] R. Heitz, M. Veit, N.N. Ledentsov, A. Hoffmann, D. Bimberg, V.M. Ustinov, P.S. Kop'ev, Z. I. Alferov, Phys. Rev. B, 56 (1997) 10435.

[67] R. Heitz, A. Kalburge, Q. Xie, M. Grundmann, P. Chen, A. Hoffmann, A. Madhukar, D. Bimberg, Phys. Rev. B, 57 (1998) 9050.

[68] K. Mukai, N. Ohtsuka, H. Shoji, M. Sugawara, Phys. Rev. B, 54 (1996) R5243.

[69] H. Yu, S. Lycett, C. Roberts, R. Murray, Appl. Phys. Lett., 69 (1996) 4087.

[70] F. Adler, M. Geiger, A. Bauknecht, F. Scholz, H. Schweizer, M.H. Pilkuhn, B. Ohnesorge, A. Forchel, Appl. Phys., 80 (1996) 4019.

[71] F. Adler, M. Geiger, A. Bauknecht, D. Haase, P. Ernst, A. Dörnen, F. Scholz, H. Schweizer, J. Appl. Phys., 83 (1998) 1631.
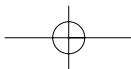
AQ1

[72] K. Brunner, U. Bockelmann, G. Abstreiter, M. Walther, G. Böhm, G. Tränkle, G. Weimann, Phys. Rev. Lett., 69 (1992) 3216.

[73] K. Kamath, H. Jiang, D. Klotzkin, J. Phillips, T. Sosnowski, T. Norris, J. Singh, P. Bhattacharya, Inst. Phys. Conf. Ser., 156 (1998) 525.

[74] T.H. Gfroerer, M.D. Sturge, K. Kash, J.A. Yater, A.S. Plaut, P.S.D. Lin, L.T. Florez, J.P. Harbison, S.R. Das, L. Lebrun, Phys. Rev. B, 53 (1996) 16474.

[75] X.-Q. Li, H. Nakayama, Y. Arakawa, Phonon Decay and Its Impact on Carrier Relaxation in Semiconductor Quantum Dots, in: D. Gershoni (Ed.) Proc. 24th Int. Conf. Phys. Semicond., World Sci., Singapore, 1998, pp. 845–848.

[76] J. Bellessa, V. Voliotis, R. Grousson, D. Roditchev, C. Gourdon, X.L. Wang, M. Ogura, H. Matsuhata, Relaxation and Radiative Lifetime of Excitons in a Quantum Dot and a Quantum Wire, in: D. Gershoni (Ed.) Proc. 24th Int. Conf. Phys. Semicond., World Scientific, Singapore, 1998, pp. 763–766.

[77] M. Lowisch, M. Rabe, F. Kreller, F. Henneberger, Appl. Phys. Lett., 74 (1999) 2489.

[78] I. Gontijo, G.S. Buller, J.S. Massa, A.C. Walker, S.V. Zaitsev, N.Y. Gordeev, V.M. Ustinov, P.S. Kop'ev, Jpn. J. Appl. Phys., 38 (1999) 674.

[79] X.-Q. Li, H. Nakayama, Y. Arakawa, Jpn. J. Appl. Phys., 38 (1999) 473.

[80] K. Kral, Z. Khas, Phys. Status Solidi. B, 208 (1998) R5.

[81] V.I. Klimov, D.W. McBranch, Phys. Rev. Lett., 80 (1998) 4028.

[82] D. Bimberg, N.N. Ledentsov, M. Grundmann, R. Heitz, J. Boehrer, V.M. Ustinov, P.S. Kop'ev, Z.I. Alferov, J. Lumin., 72–74 (1997) 34.

[83] U. Woggon, H. Giessen, F. Gindele, O. Wind, B. Fluegel, N. Peyghambarian, Phys. Rev. B, 54 (1996) 17681.

[84] M. Grundmann, R. Heitz, N. Ledentsov, O. Stier, D. Bimberg, V.M. Ustinov, P.S. Kop'ev, Z.I. Alferov, S.S. Ruvimov, P. Werner, U. Gösele, J. Heydenreich, Superlattices Microstruct. 19 (1996) 81.

[85] V.S. Williams, G.R. Olbright, B.D. Fluegel, S.W. Koch, N. Peyghambarian, J. Modern Optics, 35 (1988) 1979.

[86] B. Ohnesorge, M. Albrecht, J. Oshinowo, A. Forchel, Y. Arakawa, Phys. Rev. B, 54 (1996) 11532.

[87] G. Wang, S. Fafard, D. Leonard, J.E. Bowers, J.L. Merz, P.M. Petroff, Appl. Phys. Lett., 64 (1994) 2815.

[88] J.H.H. Sandmann, S. Grosse, G. von Plessen, J. Feldmann, G. Hayes, R. Phillips, H. Lipsanen, M. Sopanen, J. Ahopelto, Phys. Status Solidi. B, 204 (1997) 251.

[89] R. Heitz, M. Veit, A. Kalburge, Q. Xie, M. Grundmann, P. Chen, N.N. Ledentsov, A. Hoffmann, A. Madhukar, D. Bimberg, V.M. Ustinov, P.S. Kop'ev, Z.I. Alferov, Physica E (Amsterdam)., 2 (1998) 578.

[90] X.-Q. Li, Y. Arakawa, Phys. Rev. B, 57 (1998) 12285.

[91] T.S. Sosnowski, T.B. Norris, H. Jiang, J. Singh, K. Kamath, P. Bhattacharya, Phys. Rev. B, 57 (1998) R9423.

[92] R.D.J. Miller, G. McLendon, A.J. Nozik, W. Schmickler, F. Willig, Surface Electron Transfer Processes, VCH Publishers, New York, 1995.

[93] A. Meier, D.C. Selmarten, K. Siemoneit, B.B. Smith, A.J. Nozik, J. Phys. Chem. B, 103 (1999) 2122.
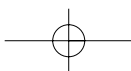
[94] A. Meier, S.S. Kocha, M.C. Hanna, A.J. Nozik, K. Siemoneit, R. Reineke-Koch, R. Memming, J. Phys. Chem. B, 101 (1997) 7038.

[95] S.J. Diol, E. Poles, Y. Rosenwaks, R.J.D. Miller, J. Phys. Chem. B, 102 (1998) 6193.

[96] R.D. Schaller, V.M. Agranovich, V.I. Klimov, Nat. Phys., 1 (2005) 189.

[97] K. Mukai, M. Sugawara, The Phonon Bottleneck Effect in Quantum Dots, in: R.K. Willardson, E.R. Weber (Eds.), Semiconductors and Semimetals, Vol 60, Academic Press, San Diego, 1999, p. 209.

[98] B.N. Murdin, A.R. Hollingworth, M.Kamal-Saadi, R.T. Kotitsche, C.M. Ciesla, C.R. Pidgeon, P.C. Findlay, H.A. Pellemans, C.J.G.M. Langerak, A.C. Rowe, R.A. Stradling, E. Gornik, Suppression of LO phonon scattering in "quasi" quantum dots, in: D. Gershoni (Ed.) Proc. 24th Int. Conf. Phys. Semicond., World Scientific, Singapore, 1998, pp. 1867–1870.

[99] L. Langof, E. Ehrenfreund, E. Lifshitz, O.I. Micic, A.J. Nozik, J. Phys. Chem. B, 106 (2002) 1606.

[100] O.I. Micic, A.J. Nozik, E. Lifshitz, T. Rajh, O.G. Poluektov, M.C. Thurnauer, J. Phys. Chem., 106 (2002) 4390.

[101] M. Shim, P. Guyot-Sionnest, Nature, 407 (2000) 981.

[102] M. Shim, C. Wang, P.J. Guyot-Sionnest, J. Phys. Chem., 105 (2001) 2369.

[103] A.L. Efros, A.J. Nozik, J. Phys. Chem. B, (2003) to be published.

[104] H.K. Jung, K. Taniguchi, C. Hamaguchi, J. Appl. Phys., 79 (1996) 2473.

[105] D. Harrison, R.A. Abram, S. Brand, J. Appl. Phys., 85 (1999) 8186.

[106] J. Bude, K. Hess, J. Appl. Phys., 72 (1992) 3554.

[107] V.S. Vavilov, J. Phys. Chem. Solids, 8 (1959) 223.

[108] J. Tauc, J. Phys. Chem. Solids, 8 (1959) 219.

[109] R.J. Hodgkinson, Proc. Phys. Soc., 82 (1963) 1010.

[110] O. Christensen, J. Appl. Phys. 47 (1976) 690.

[111] M. Wolf, R. Brendel, J.H. Werner, H.J. Queisser, J. Appl. Phys., 83 (1998) 4213.

[112] R.D. Schaller, M.A. Petruska, V.I. Klimov, Appl. Phys. Lett., 87 (2005) 1.

[113] J.E. Murphy, M.C. Beard, A.G. Norman, S.P. Ahrenkiel, J.C. Johnson, P. Yu, O.I. Micic, R.J. Ellingson, A.J. Nozik, J. Am. Chem. Soc., (2006) in press.

[114] A.J. Nozik, (1996) unpublished manuscript.

[115] C.B. Murray, C.R. Kagan, M.G. Bawendi, Annu. Rev. Mater. Sci., 30 (2000) 545.

[116] O.I. Micic, S.P. Ahrenkiel, A.J. Nozik, Appl. Phys. Lett., 78 (2001) 4022.

[117] O.I. Micic, K.M. Jones, A. Cahill, A.J. Nozik, J. Phys. Chem. B, 102 (1998) 9791.

[118] M. Sugawara, Self-Assembled InGaAs/GaAs Quantum Dots, in: M. Sugawara (Ed.) Semiconductors and Semimetals, Vol 60, Academic Press, San Diego, 1999, pp. 1–350.

[119] Y. Nakata, Y. Sugiyama, M. Sugawara, in: M. Sugawara (Ed.) Semiconductors and Semimetals, Vol 60, Academic Press, San Diego, 1999, pp. 117–152.

[120] A. Hagfeldt, M. Grätzel, Acc. Chem. Res., 33 (2000) 269.

[121] J. Moser, P. Bonnote, M. Grätzel, Coord. Chem. Rev., 171 (1998) 245.

[122] M. Grätzel, Prog. Photovoltaics, 8 (2000) 171.

[123] A. Zaban, O.I. Micic, B.A. Gregg, A.J. Nozik, Langmuir, 14 (1998) 3153.

[124] R. Vogel, H. Weller, J. Phys. Chem., 98 (1994) 3183.

[125] H. Weller, Ber. Bunsen-Ges. Phys. Chem., 95 (1991) 1361.

[126] D. Liu, P.V. Kamat, J. Phys. Chem., 97 (1993) 10769.

AQ2

AQ3
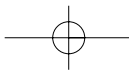
1   [127] P. Hoyer, R. Könenkamp, Appl. Phys. Lett., 66 (1995) 349.
2   [128] N.C. Greenham, X. Peng, A.P. Alivisatos, Phys. Rev. B, 54 (1996) 17628.
3   [129] N.C. Greenham, X. Peng, A.P. Alivisatos, A CdSe Nanocrystal/MEH-PPV Polymer
4   Composite Photovoltaic, in: R. McConnell (Ed.) Future Generation Photovoltaic
     Technologies: First NREL Conference, Am. Inst. Phys., 1997, p. 295.
5   [130] W.U. Huynh, X. Peng, P. Alivisatos, Adv. Mater., 11 (1999) 923.
6   [131] A.C. Arango, S.A. Carter, P.J. Brock, Appl. Phys. Lett., 74 (1999) 1698.
7   [132] B.O. Dabbousi, M.G. Bawendi, O. Onitsuka, M.F. Rubner, Appl. Phys. Lett., 66
8   (1995) 1316.
9   [133] V. Colvin, M. Schlamp, A.P. Alivisatos, Nature, 370 (1994) 354.
     [134] M.C. Schlamp, X. Peng, A.P. Alivisatos, J. Appl. Phys., 82 (1997) 5837.
10   [135] H. Mattoussi, L.H. Radzilowski, B.O. Dabbousi, D.E. Fogg, R.R. Schrock, E.L.
11   Thomas, M.F. Rubner, M.G. Bawendi, J. Appl. Phys., 86 (1999) 4390.
12   [136] H. Mattoussi, L.H. Radzilowski, B.O. Dabbousi, E.L. Thomas, M.G. Bawendi, M.F.
13   Rubner, J. Appl. Phys., 83 (1998) 7965.

14
15
16
17
18
19
20
21
22
23
24
25
26
27
28
29
30
31
32
33
34
35
36
37
38
39
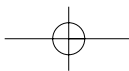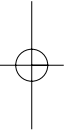
AUTHOR QUERY FORM

ELSEVIER	**Book : NMSC-SOGA** **Chapter : CH015**	**Please e-mail or fax your responses and any corrections to:** **E-mail:** **Fax:**

Dear Author,

During the preparation of your manuscript for typesetting, some questions may have arisen. These are listed below. Please check your typeset proof carefully and mark any corrections in the margin of the proof or compile them as a separate list*.

Disk use
Sometimes we are unable to process the electronic file of your article and/or artwork. If this is the case, we have proceeded by:
∈ Scanning (parts of) your article   ∈ Rekeying (parts of) your article   ∈ Scanning the artwork

∈ *Uncited references*: This section comprises references that occur in the reference list but not in the body of the text. Please position each reference in the text or delete it. Any reference not dealt with will be retained in this section.

Queries and / or remarks

Location in Article	Query / remark	Response
AQ1	In Ref.[50], please provide the name of the editor.	
AQ2	Please update Ref.[103], if data are available.	
AQ3	Please update Ref. [113], if data are available	

Thank you for your assistance